



A novel slurry concept for the fabrication of lithium-ion battery electrodes with beneficial properties



Boris Bitsch^{a,*}, Jens Dittmann^a, Marcel Schmitt^b, Philip Scharfer^b, Wilhelm Schabel^b, Norbert Willenbacher^a

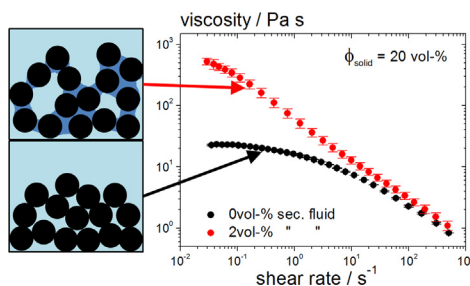
^aKarlsruhe Institute of Technology, Institute for Mechanical Process Engineering and Mechanics, Gotthard-Franz-Str. 3, 76131 Karlsruhe, Germany

^bKarlsruhe Institute of Technology, Institute of Thermal Process Engineering, Thin Film Technology, Kaiserstr. 12, 76131 Karlsruhe, Germany

HIGHLIGHTS

- We present a new slurry concept based on capillary suspensions for Li-ion electrodes.
- The slurry viscosity in the low shear region is tunable in a wide range without further additives.
- The slurry viscosity in the high shear region remains unchanged which is desirable during coating.
- Storage stability and shape accuracy during coating are improved significantly.
- Good mechanical and electrochemical properties of the novel electrodes are shown.

GRAPHICAL ABSTRACT



ARTICLE INFO

Article history:

Received 9 October 2013
Received in revised form
4 April 2014
Accepted 23 April 2014
Available online 2 May 2014

Keywords:

Lithium-ion batteries
Capillary suspension
Electrode processing
Slurry viscosity
Flow properties

ABSTRACT

A novel slurry concept for the fabrication of Li-ion battery electrodes focusing on water based formulations is presented. Taking advantage of capillary forces inferred by adding a small fraction of a second fluid immiscible with the bulk continuous phase the low shear viscosity can be varied in a wide range without conventional polymeric rheology control agents disturbing the electric properties of the dry electrode. The new slurries provide superior storage stability and excellent shape accuracy of the final dry film. This reduces waste cut-off at the edges and increases the density of active ingredients, thus improving cost-efficiency. The viscosity at high shear rates remains unaffected, thus the slurries can be processed and coated using established equipment and process parameters. Adhesion to the conductor foil and electrochemical properties of the electrode layers and corresponding cells are similar to those made from conventional slurries.

© 2014 Elsevier B.V. All rights reserved.

1. Introduction

The performance of lithium-ion batteries is strongly dependent on the electrochemical characteristics and the fraction of active material in the electrodes. However, the fabrication process also plays an important role since it determines the distribution of active material and the structure of the electrode layers.

* Corresponding author. Tel.: +49 721 60848824; fax: +49 721 60843758.
E-mail address: boris.bitsch@kit.edu (B. Bitsch).

Optimization of the fabrication process leads to the cheaper production of electrodes with improved properties like capacity, cycleability, safety, toxicity and cost [1].

Typically, slurries for lithium-ion electrodes consist of a solvent, the anode or cathode active material, carbon black to ensure the electrical conductivity and a binder for the cohesion between the particles and the adhesion of the electrode layer to the current collector respectively. Furthermore, water based slurries generally contain rheology control agents to adjust the flow properties according to the demands of the respective coating operations.

In general, the process chain for electrode manufacturing is distinguished by its complexity and the large number of influencing factors: the first step is the dispersion of the solids in the solvent to receive a processible and homogenous slurry. This slurry is coated in the subsequent step on the current collector followed by the drying and calendaring of the electrode layer. The chosen technology and parameters for mixing and coating as well as the drying and calendaring [2] conditions determine the slurry homogeneity, the electrode thickness, the mechanical stability or the porosity of the electrode layer. Therefore, the electrode processing has direct influence on the electrode performance. Beyond that, the characteristics of the chosen active material and additives, the mixing sequences, ingredient ratios and potential additional pretreatment steps of the solids (e.g. dry mixing) have also a strong effect on the electrode performance [1].

The electrode slurry plays a central role in the fabrication process: the flow behavior of the slurry is determined by the ratio of raw materials, the mixing procedure and the mixing sequence. Furthermore, the viscosity function and the sedimentation stability of electrode slurries are factors with superior relevance to the subsequent coating process [3].

Although there are several publications related to the processing of lithium-ion electrodes, the literature focusing on rheological properties of electrode slurries and its optimization is scarce. Kim et al. [4] and Lee et al. [5] discussed the effects of different mixing sequences on the rheological properties of NMP-based cathode slurries and its consequences on the dried electrode. In aqueous anode slurries, Lee et al. investigated the influence of sodium carboxymethylcellulose (CMC) focusing on concentration and degree of substitution [6]; further Lee et al. examined the slurry viscosity depending on the fractions of styrene butadiene rubber (SBR) and CMC [7]. With rising CMC concentration the slurry viscosity increases drastically whereas the addition of SBR does not have a significant effect on the flow properties of the slurry. Beside its major effect on the slurry rheology, CMC also contributes to the mechanical stability of dry electrodes [8].

In the present work, we introduce an innovative slurry concept for the fabrication of lithium-ion electrodes based on capillary suspensions. By adding a small amount (~ 1 vol%) of a secondary fluid, that is immiscible with the primary fluid, the flow properties of the suspension can be changed drastically [9]. This general physical phenomenon is found in various kinds of material systems [10]. By adding a secondary fluid to a suspension, an existing sample-spanning network (e.g. van-der-Waals) may be reinforced or such a network is created due to capillary forces introduced by the secondary fluid [11,12]. The corresponding change in flow properties can be utilized to match the specific needs of a certain downstream process unit, in our case the coating of the electrode slurry on the metallic current collector foil.

The coating of homogenous films with constant layer thickness is a key challenge for industrial electrode fabrication. But not only a constant thickness at the center of the electrode layer needs to be achieved, also the shape of the sidewise edges plays an important role. Blurred edges have to be cut-off in order to guarantee for a constant amount of active material per unit area. However, at the

position of the take-off lug the edge cannot be cut-off and may lead to a local excess voltage due to the reduced amount of active material at this point. Moreover, depending on slurry rheology and coating conditions local superelevations at the layer curb, so-called “heavy edges”, may occur with major disadvantages for the subsequent fabrication steps.

Superelevations lead to inhomogeneous pressure distributions during calendaring resulting in a non-uniform porosity and area capacity of the electrode. Furthermore, regarding production on industrial scale, up-winding of hundreds of electrode layers superelevations add up to several millimeters and provoke undesirable folds in the electrode foil [13]. For these reasons, a good accuracy of the edge shape is of superior importance for industrial electrode processing.

Here, we want to evaluate the novel slurry concept based on capillary suspensions as a cost saving fabrication method for industrial electrode production. We target on an increase of the slurry viscosity at low shear rates in order to fabricate layers with superior coating properties, i.e. sharper edge contours; finally aiming at a reduction of cut-off waste and therefore lower production costs. Furthermore, the concept shall be used to improve sedimentation stability of the slurry. The utilized secondary fluid evaporates during coating and does not remain in the dry electrode layer. The capillary suspension concept is intended to enable a reduction of organic additives like rheological additives and binders, thus allowing higher active material density and better electric conductivity of the electrode layer. Due to similar viscosity data of capillary suspensions at high shear rates in comparison to conventional slurries the application of established coating equipment is possible.

Capillary forces control the formation and strength of the network based on secondary fluid bridges between the particles. The three-phase contact angle $\theta_{S,B}$ is defined as the angle of the secondary phase (S) against the solid surface while surrounded by the bulk fluid (B). Depending on $\theta_{S,B}$, two general states can be distinguished: if $\theta_{S,B} > 90^\circ$ the secondary phase does not preferentially wet the particles and therefore forms droplets surrounded

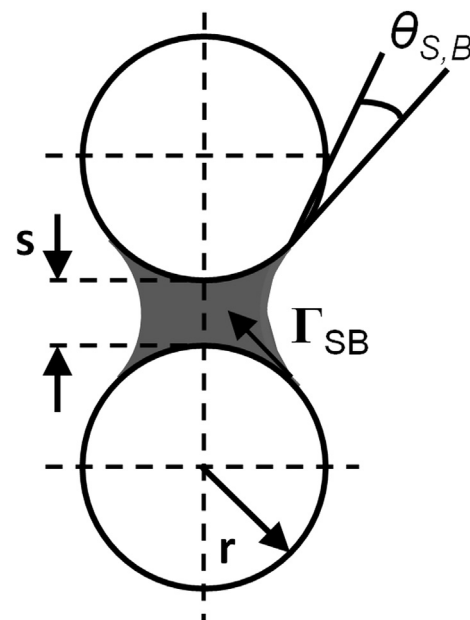


Fig. 1. Schematic drawing of two spherical solid particles connected by a liquid drop in the pendular state giving the essential parameters. The contact angle $\theta_{S,B}$ determines if the admixture is in the pendular state ($\theta_{S,B} < 90^\circ$) or capillary state ($\theta_{S,B} > 90^\circ$).

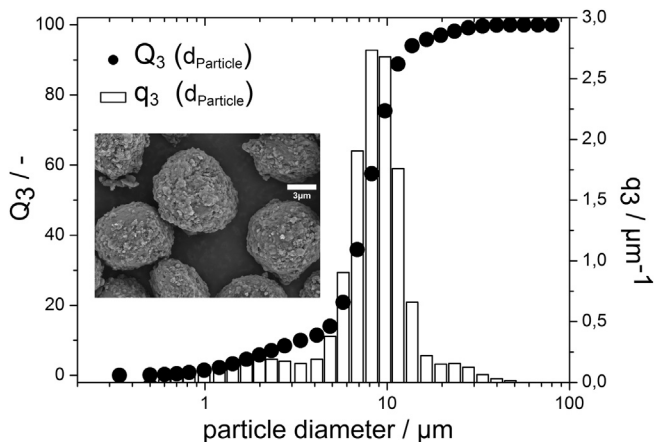


Fig. 2. Particle size distribution and SEM image of the used graphite powder. Q_3 and q_3 represent the cumulated and differential particle size distribution determined by Fraunhofer diffraction.

by particle clusters which then form a sample-spanning network [11]. In analogy to wet granular media this is called the capillary state, but it should be kept in mind that the particle loading is typically low and particles are by far not densely packed. In contrast to so-called Pickering emulsions the fluid volume trapped by these clusters is typically smaller than the particle volume. If $\theta_{S,B} < 90^\circ$, the secondary fluid preferentially wets the particle surface and forms liquid bridges between particles. The corresponding network structure of the suspension is termed pendular state. The expanded Young–Dupré equation is used to calculate the three-phase contact angle $\theta_{S,B}$ [14–16]

$$\cos \theta_{S,B} = \frac{\Gamma_{Sa} \cos \theta_{S,a} - \Gamma_{Ba} \cos \theta_{B,a}}{\Gamma_{SB}} \quad (1)$$

where $\theta_{i,a}$ stands for the contact angle of the considered fluid against the solid surface in air (a) and $\Gamma_{i,a}$ is the surface tension of the fluid against air. In Fig. 1, a two-sphere model exemplarily shows the relevant factors for the strength of a capillary bridge. The force F_C acting between two spherical particles of radius r connected by a capillary bridge is given by:

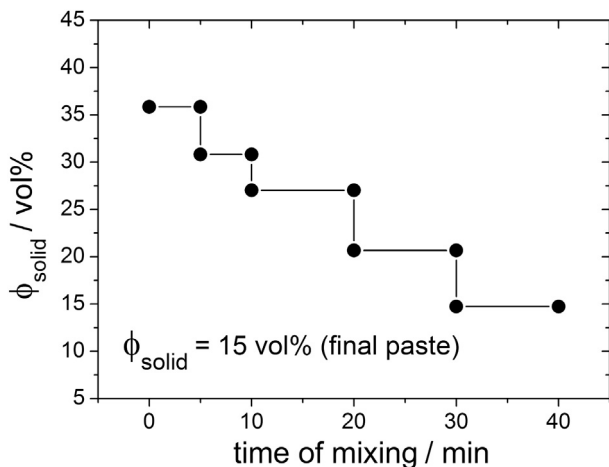


Fig. 3. Mixing procedure given as solid volume fraction over mixing time (exemplarily given for the 15 vol% slurry). Starting from high solid fractions water is stepwise added during the dissolver mixing process in order to guarantee for a good deagglomeration of solid particles.

$$F_C = g(V, s) \Gamma_{SB} r \cos \theta_{S,B} \quad (2)$$

where Γ_{SB} is the interfacial tension between bulk and secondary phase [17]. The capillary force is proportional to Γ_{SB} . The function g further depends on the volume of the capillary bridge V and the particle surface separation s . If the capillary bridge is small compared to the particle radius equation (Eq. (2)) reduces to [9]:

$$F_C = 2\pi \Gamma_{SB} r \cos \theta_{S,B} \quad (3)$$

It should be noted that the capillary force acting between particles is typically two orders of magnitude stronger than the ubiquitous van-der-Waals force. This corresponds to a higher network strength and high yield stresses of capillary suspensions compared to flocculated suspensions where van-der-Waals forces control network formation.

In this work, we have systematically examined the use of capillary suspensions as aqueous anode slurries. Their flow properties and benefits for the electrode layer are thoroughly discussed. A transfer of this slurry concept to cathode slurries is dedicated to future research.

2. Experimental

2.1. Material system

Commercially available spherical, synthetic graphite particles (China Steel Chemical Corporation, Kaohsiung, Taiwan) with a volume-based average diameter $d_{50,3}$ of 7.8 μm , an almost monomodal size distribution (Fig. 2), a specific surface area of less than 3.2 $\text{m}^2 \text{g}^{-1}$ and a density of 2.2 g cm^{-3} were used as the active ingredient of the aqueous anode slurries investigated here. Carbon black (CB, Super C65, TIMCAL, Bodio, Switzerland) with a density of 1.8 g cm^{-3} was added as conductivity agent. The size of the primary CB particles is about 30 nm, but in the slurry they are present as aggregates with an average size of several microns [18]. The binder was supplied as an aqueous styrene butadiene rubber (SBR) dispersion (JSR Corporation, Tokyo, Japan) with a density of about 1.0 g cm^{-3} and a solid mass fraction of 48%. CMC (Daicel Corporation, Osaka, Japan) with an average molecular weight of 1,400,000–1,500,000 g mol^{-1} , a density of 1.59 g cm^{-3} and a degree of substitution of >0.8 was added as binding agent and as rheology control agent. As secondary fluid 1-octanol (Alfa Aesar, Karlsruhe, Germany) with a density of 0.83 g cm^{-3} and dynamic viscosity of 0.009 Pa s at 20 $^\circ\text{C}$ was added to the suspension. The ratio of solids to liquids was varied throughout the experiments between 15 and 25 vol% whereas the weight ratio of graphite to CB to CMC to SBR was kept constant at 93:2:2.5:2.5.

2.2. Processing route

The processing route is composed of mixing and coating the slurry, drying and calendaring the electrode layer and assembling the cell. CMC was dissolved in water (3wt-% CMC– H_2O mixture) and initially mixed with all solids except the SBR dispersion using a dissolver stirrer at 1200 rounds per minute (rpm) for 30 min. In order to guarantee for a good deagglomeration and slurry homogeneity, a highly concentrated suspension was initially mixed while the amount of liquid was raised stepwise with time as shown in Fig. 3 [5]. After this first mixing step, two different mixing sequences were employed to fabricate the reference slurry and the slurry based on a capillary suspension (Fig. 4). In the reference slurry, SBR was added to the premixed suspension using a dissolver mixer at only 800 rpm. For the capillary suspension, the secondary

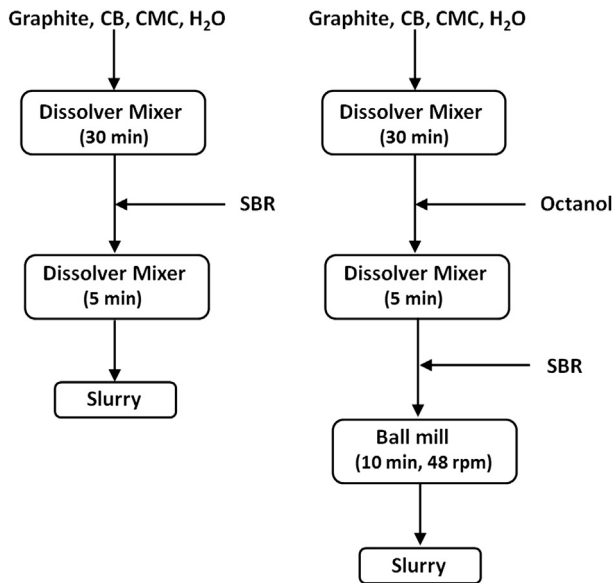


Fig. 4. Schematic drawing of the slurry preparation processes: preparation of a slurry without added secondary fluid (left) and with added secondary fluid (right).

fluid was at first added to the premixed suspension followed by dissolver mixing at 800 rpm. The network formation was controlled by torque measurements. Afterwards, the SBR was added to the capillary suspension using a ball mill at 48 rpm for 10 min. For the analysis of the mechanical strength of dry electrodes, both slurry systems were coated onto a 10 μm thick copper foil (Itochu Corporation, Tokyo, Japan) applying a ZUA 2000 doctor blade (Zehntner GmbH, Sissach, Switzerland) with a coating width of 60 mm and a coating gap of 300 μm . The wet film was dried for 20 min at 130 $^{\circ}\text{C}$ and overnight at room temperature. Finally, the adhesion of the dry film to the copper foil was characterized by peel-test measurements.

For the determination of the electrode edge contour slot die coating was employed as coating method. The thickness of the slot die upstream, downstream and side lip were constant: $L_U = L_D = L_S = 500 \mu\text{m}$. The slot width is defined by a die-shim with a thickness of $S = 500 \mu\text{m}$ while the coating gap was adjusted to

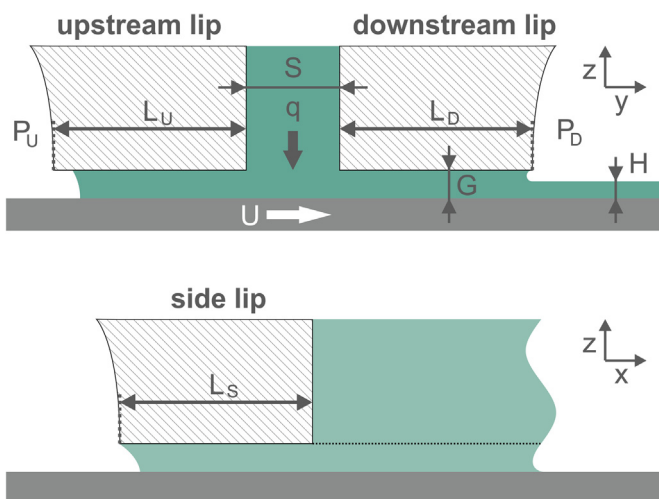


Fig. 5. Two-dimensional sketch of the slot die's cross-section in coating direction (top) and in cross-web direction (bottom).

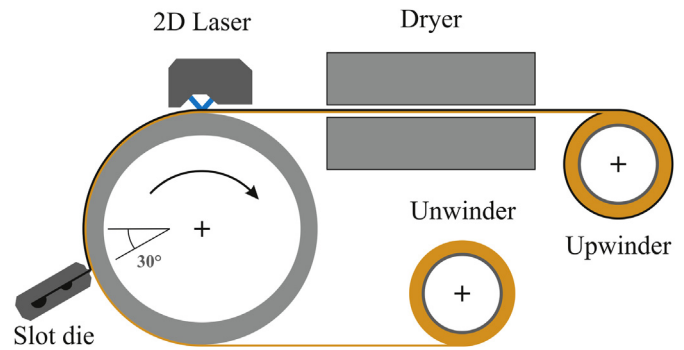


Fig. 6. Schematic drawing of the experimental set-up to determine edge contours via laser triangulation subsequent to slot die coating and before drying the electrode layer.

$G = 180 \mu\text{m}$ (see Fig. 5). The 60 mm wide and 172 μm thick wet film was dried for 20 min at 130 $^{\circ}\text{C}$ and overnight at room temperature in an ambient atmosphere. For cell testing, the electrode layers were calendared applying a force of 80 kN at 60 $^{\circ}\text{C}$, then dehumidified in a dry room overnight. Electrochemical tests were carried out, firstly using a three-electrode EL-Cell configuration (EL-Cell GmbH, Hamburg, Germany). Processed anodes (18 mm diameter) were assembled in a dry argon-filled glove box using EL-Cell glass fiber membranes (thickness: 1.55 mm, Whatman, Maidstone, UK) as separator, LP30 as electrolyte (BASF, Ludwigshafen, Germany) and lithium foil (0.38 mm thickness from Sigma-Aldrich, St. Louis, USA) as counter and reference electrode. Secondly, two-electrode Swagelok half cells were assembled in a dry argon-filled glove box using the processed anodes (11 mm diameter), glass fiber membranes (thickness: 200 μm , Whatman, Maidstone, UK) as separator, LP30 as electrolyte and lithium foil (12 mm diameter, 0.75 mm thickness from VWR International GmbH, Darmstadt, Germany) as counter-electrode. Finally, full cells were fabricated in a dry room as pouch cells (50 mm \times 50 mm). The utilized counter Lithium–Nickel–Cobalt–Manganese oxide (NMC) cathode, ceramic separator with a thickness of 30 μm and the electrolyte LP 30 are state-of-the-art products supplied by industrial partners.

2.3. Characterization methods

The particle size distribution was determined by Fraunhofer diffraction (Sympatec, Helos H0309, Clausthal-Zellerfeld, Germany) with a wet dispersing unit (Sympatec Quixel, Clausthal-Zellerfeld, Germany). Densities of solid materials were determined applying helium pycnometry (Micromeritics, Multi Volume Pycnometer, Aachen, Germany). Rheological properties of the basic fluids and slurries were measured using a stress-controlled rotational rheometer (RheoStress 1, Thermo Scientific, Karlsruhe, Germany) with a cone/plate (diameter: 60 mm, angle: 1 $^{\circ}$) and a plate/plate (diameter: 35 mm, gap height: 1 mm) geometry. The viscosity functions were determined applying shear stress ramps (initial stress: 0.5 Pa or 1.0 Pa, final stress: 500 Pa or 1000 Pa, measurement time: 300 s). For oscillatory shear measurements, the linear viscoelastic range was initially determined using stress sweeps at two fixed frequencies (1.0 and 10 rad s^{-1}). Afterwards, the storage and loss moduli were determined by frequency sweeps (from 0.07 to 100 rad s^{-1}) at stress amplitudes within the linear viscoelastic range (0.7 and 1.0 Pa). The surface and interfacial tension were measured using a weight-based Tensiometer (Dataphysics, DCAT 11, Filderstadt, Germany) with a Wilhelmy plate geometry. The contact angle was determined using the sessile drop method (Dataphysics, OCA15, Filderstadt, Germany). During slot die coating



Fig. 7. Characteristic texture of anode slurries ($\phi_{\text{total}} = 20 \text{ vol}\%$: graphite, CB and CMC in water; the ratio of graphite to CB to CMC is 95.4:2.0:2.6) with different amounts of secondary fluid octanol as indicated above.

the edge geometry was detected via a two-dimensional laser triangulation system (LJ-V7060, Keyence, Osaka). According to the schematic drawing in Fig. 6, the laser is positioned behind the coating machine and detects the edge region of the layer. Further, the surface weight as well as the film thickness of the dried electrode were measured. Both values together with the mean density of the dry layer were used to estimate the electrode porosity [2]. The complete evaporation of octanol after drying has been verified gravimetrically with an accuracy of 0.8%. A precision balance was used to compare the weight of electrode layers before and after heating to 200 °C. The adhesion of the electrode layer to the current collector was investigated by a 90°-peel-test (according to DIN 28510-1) using a TA.XT plus Texture Analyzer (Stable Micro Systems, Godalming, UK). Electrode layers with a width of 25 mm and

a length of 70 mm were investigated by peel testing at a pre-selected peel velocity and the resulting peel force was measured. The peel velocity had negligible influence on the measured peel force and was kept constant at 5 mm s⁻¹. A 5 kg load cell force sensor (max. force: 5 kg, force sensitivity: 0.1 g) was applied for all peel-tests. Samples of dry electrode edge-regions were vacuum infused with epoxy resin, grinded with SiC paper and polished with a diamond suspension (Buehler, Düsseldorf, Germany) for crosscut scanning electron microscopy (SEM) images. These images were taken in backscattering mode (Hitachi, S-4500, Krefeld, Germany). All fabricated cells were investigated applying constant current/constant voltage charging and constant current discharging at 20 °C. The three-electrode EL-cells were tested utilizing a 100-channel Maccor Series 4000 cell tester (Maccor Inc., Tulsa, USA), whereas Swagelok and pouch cells were both tested using a 64-channel cell tester (Arbin BT 2000, Hamburg, Germany). Anodes in EL-cells and Swagelok half cells against lithium were investigated applying varied charge/discharge rates for three cycles per charge/discharge rate. The cut-off potentials were set at 1.5 V and 5 mV.

In addition, the cycle stability was characterized in full cells testing anodes against commercially available NMC-cathodes. To guarantee for a complete solid electrolyte interphase (SEI) formation, the cells were initially loaded at a C/10 rate and five times cycled at a C/2 rate whereas the cut-off potentials were set at 3.0 and 4.2 V. Cell tests were performed at 1C–1C charge/discharge rates for 100 cycles.

3. Results and discussion

Surface tension and interfacial tension of aqueous CMC solutions against octanol are essentially independent of CMC concentration since the large CMC molecules are not surface active. For the surface tension of the CMC solutions we find 72.4 mN m⁻¹, which is close to the value for pure water. The surface tension of octanol is

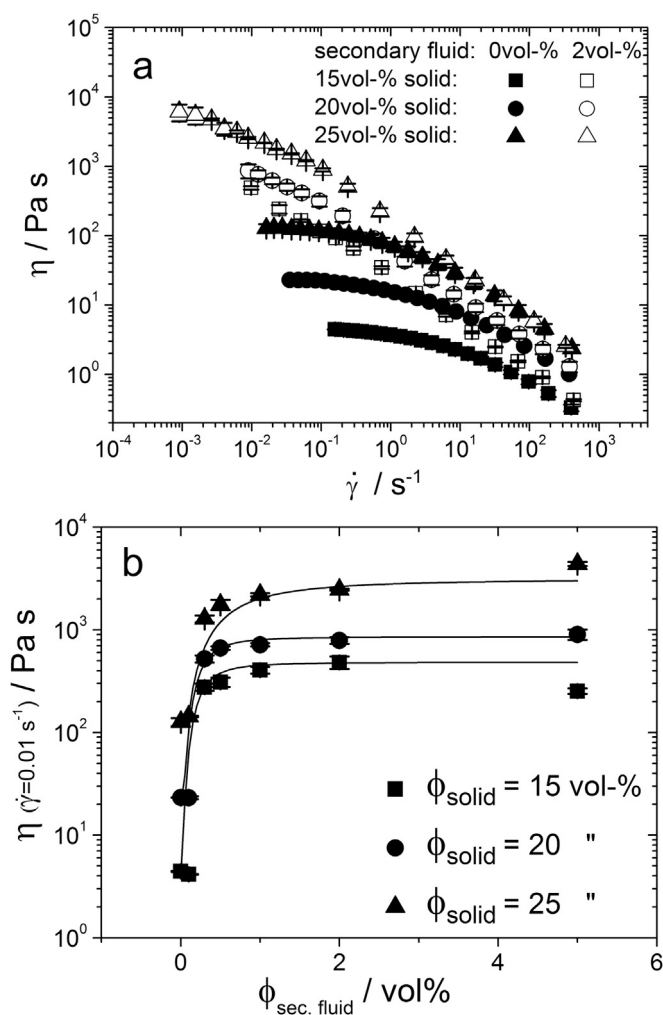


Fig. 8. Viscosity curves (a) and low shear viscosity data (b) (symbols with error bars) for slurries containing different solid fractions and varied fractions of secondary fluid (without SBR addition).

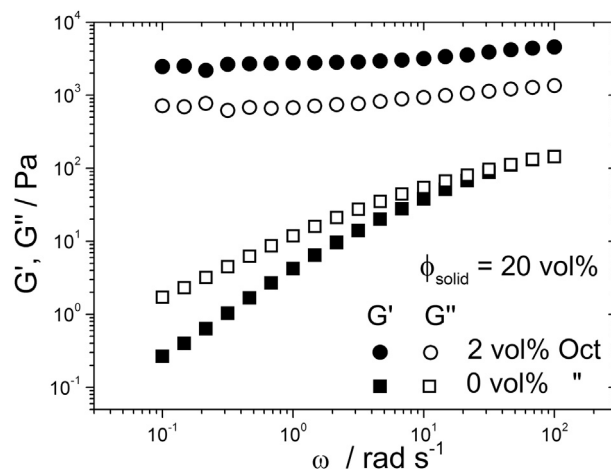


Fig. 9. Storage and loss modulus for a slurry containing 2 vol% of secondary fluid and a slurry without secondary fluid at a constant solid fraction ($\phi_{\text{solid}} = 20 \text{ vol}\%$).

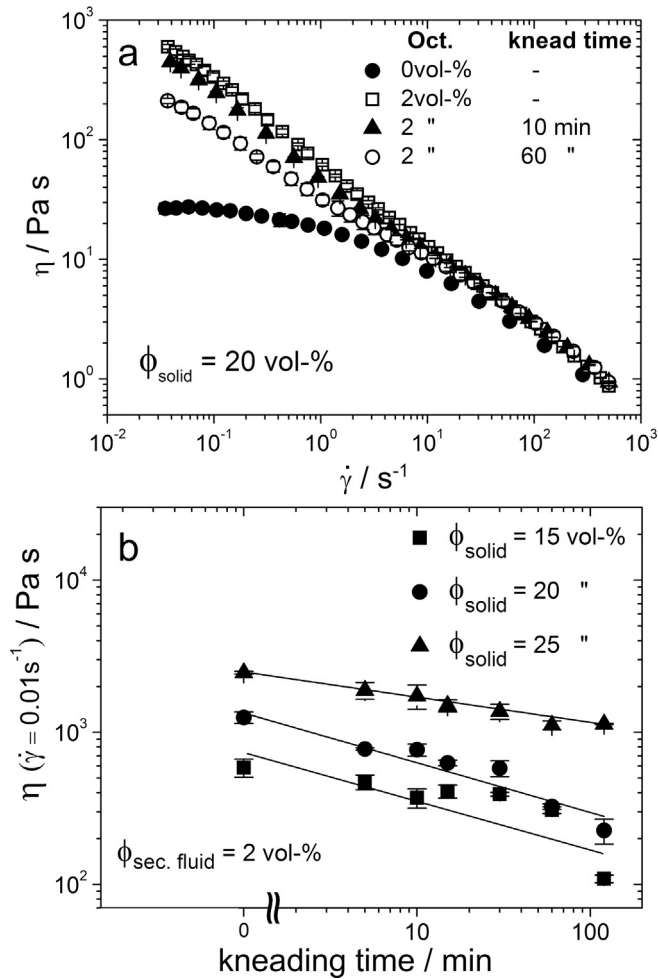


Fig. 10. Viscosity curves (a) and low shear viscosity data (b) for slurries after SBR addition and varied kneading times.

27.3 mN m^{-1} and the interfacial tension between the CMC solutions and octanol is 10.6 mN m^{-1} . The contact angle for the CMC

solutions on graphite in air is 74° , while octanol completely wets the graphite particles ($\theta_{S,a} = 0^\circ$). This results in a three-phase contact angle of $\theta_{S,B} = 46^\circ$ and we conclude that capillary suspensions based on graphite and water with octanol as secondary fluid are in the pendular state. In this study, octanol was used as secondary fluid, immiscible with water. In case octanol would have undesirable interactions with the electrode active material, it can be replaced by other volatile, hydrophobic organic liquids.

3.1. Influence of the mixing technique on the slurry flow properties

Dissolver mixing was found to be inappropriate for the SBR addition to the capillary suspension since with this mixing technique the network strength was reduced significantly before reaching a homogeneously mixed state. This might be due to the destruction of capillary bridges at high rotational speed in the dissolver mixer followed by the covering of the graphite surface through SBR polymers. This in turn prevents the reformation of a stable network of capillary bridges after the stirring process stops. By applying a ball mill at low speed, i.e. low energy input during mixing, the destruction of the capillary network was mostly prevented.

3.2. Rheological characterization

In Fig. 7, the texture of capillary anode slurries with a constant volume fraction of $\phi = 20 \text{ vol-\%}$ and different amounts of secondary fluid is shown. The suspensions without and with a marginal amount of added secondary fluid, respectively (0 vol% and 0.1 vol%) spread like dilute suspensions. Adding a slightly larger amount of secondary fluid (0.3 vol%) results in a drastic change of texture and a rather paste-like behavior, i.e. the low shear viscosity increases drastically due to the creation of a sample-spanning particle network induced by capillary forces. With further addition of secondary fluid (from 0.5 vol% to 5 vol%), the suspensions become more and more gel-like or paste-like which implies improved sedimentation stability. Fig. 8a displays the viscosity as a function of the shear rate for anode slurries containing 2 vol% octanol and slurries without secondary fluid. The solid volume fraction was varied for both slurry types between 15 vol% and 25 vol%.



Fig. 11. Electrode section before (top) and after (bottom) peel-testing.

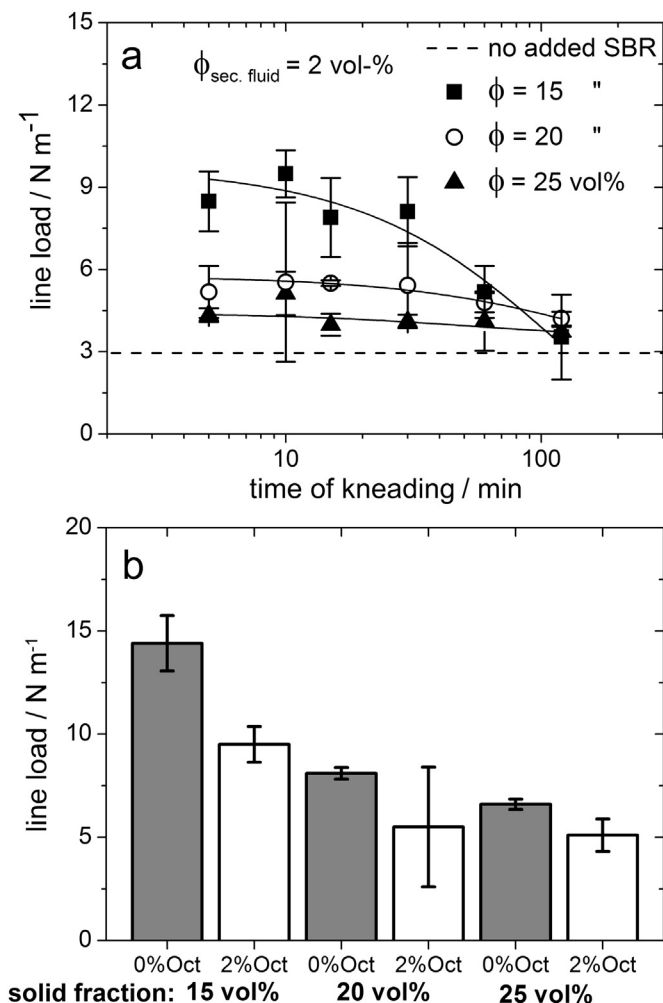


Fig. 12. Line load derived from peel-test as function of kneading time after SBR addition for slurries with addition of 2 vol% octanol and varied solid fraction (a). Line load comparison for conventional slurries without added octanol and capillary suspensions with 2 vol% added SBR, 10 min kneaded and varied solid fraction (b).

A strong decrease in viscosity with increasing shear rate can be observed even at these intermediate concentrations for both electrode slurry types indicating that attractive interactions among particles are present. However, adding an amount of 2 vol% octanol

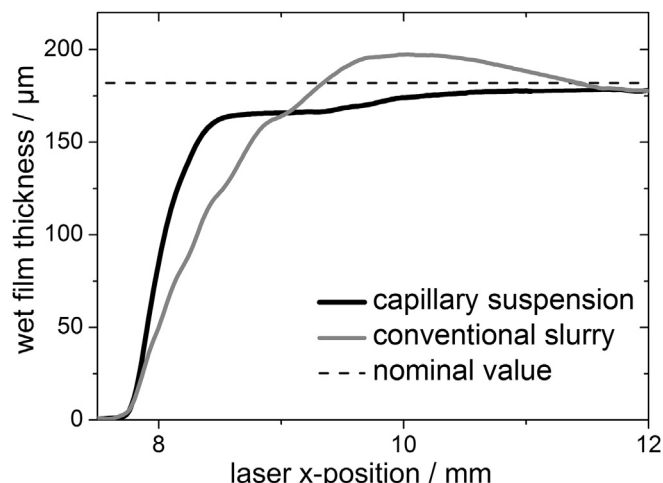


Fig. 13. Edge contour of wet, coated slurries determined via laser triangulation.

to the suspension leads to a drastic increase in the low shear viscosity which is due to the formation of a strong network induced by capillary forces. Remarkably, the viscosity at high shear rates of such capillary anode slurries is similar compared to samples without secondary fluid (Fig. 8a). Obviously, the capillary network breaks down when high shear forces are applied. When decreasing the shear force the capillary network recovers quickly as the viscosity data obtained from subsequent stress ramps taken after 1 min waiting time coincide.

Viscosity at a low shear rate of $\dot{\gamma} = 0.01 \text{ s}^{-1}$ is shown in Fig. 8b as a function of the secondary fluid fraction for differing solid contents. The viscosity at this low shear rate increases with rising amount of secondary fluid by at least one order of magnitude. Similar results have been reported for various other material systems [9–12,19]. At a secondary fluid fraction of 0.5 vol%, a plateau value in the low shear viscosity is reached indicating that network formation is completed and larger amounts of secondary fluid do not further change structure and flow properties. For the sample with the lowest particle loading, the low shear viscosity even drops slightly when 5 vol% of secondary fluid is added compared to the 2 vol% sample. This might be due to the formation of compact agglomerates immobilizing less fluid as observed for ceramic capillary suspensions [19].

The drastic change in flow properties after adding minor amounts of secondary fluid is also obvious from oscillatory shear measurements. In Fig. 9, the storage modulus (G') and the loss modulus (G'') are shown as a function of the angular frequency for two anode slurries, both composed of 20 vol% solids. For the slurry without secondary liquid both moduli show a frequency dependence and G'' is consistently higher than G' . Therefore, the slurry behavior can be characterized as a well-dispersed sol [5]. By adding 2 vol% of octanol a sample-spanning network is created which strongly affects the viscoelastic properties. A frequency dependency of G' and G'' is no longer observable and the storage modulus G' dominates over the loss modulus G'' , i.e. the slurry exhibits gel-like behavior.

These observations demonstrate that the formation of a capillary suspension affects greatly the low shear viscosity but has minor influence on the flow properties at high shear rates.

After the formation of the sample-spanning network the addition of the SBR binder was carried out using a ball mill. In Fig. 10a, the viscosity is shown as a function of shear rate for the basic slurry containing neither secondary fluid nor SBR, the corresponding capillary suspension including 2 vol% octanol and the complete suspension after addition of SBR at different kneading times in the ball mill. With the addition of secondary fluid the low shear viscosity increases drastically. But during kneading the SBR binder into the capillary suspension the low shear viscosity drops monotonically with increasing kneading time as shown in Fig. 10b. This phenomenon can be explained with the change in interfacial properties due to the SBR addition. The used SBR is an aqueous polymer dispersion stabilized by minor amounts of surfactant. By adding 1 vol% of SBR to a 1 wt% CMC–water solution the interfacial tension against octanol decreases from 10.6 to 7.8 mN m⁻¹ which results in lower capillary forces and therefore a weaker capillary network. Finally, we conclude that the kneading time is another parameter to adjust rheological properties of anode slurries based on capillary suspensions with added SBR binder.

3.3. Characterization of mechanical properties

The adhesion force between anode layer and copper foil was analyzed using a 90°-peel-test. Fig. 11 shows an electrode before testing and the copper foil surface after peeling which proves that the peel test is qualified to determine the adhesion strength since

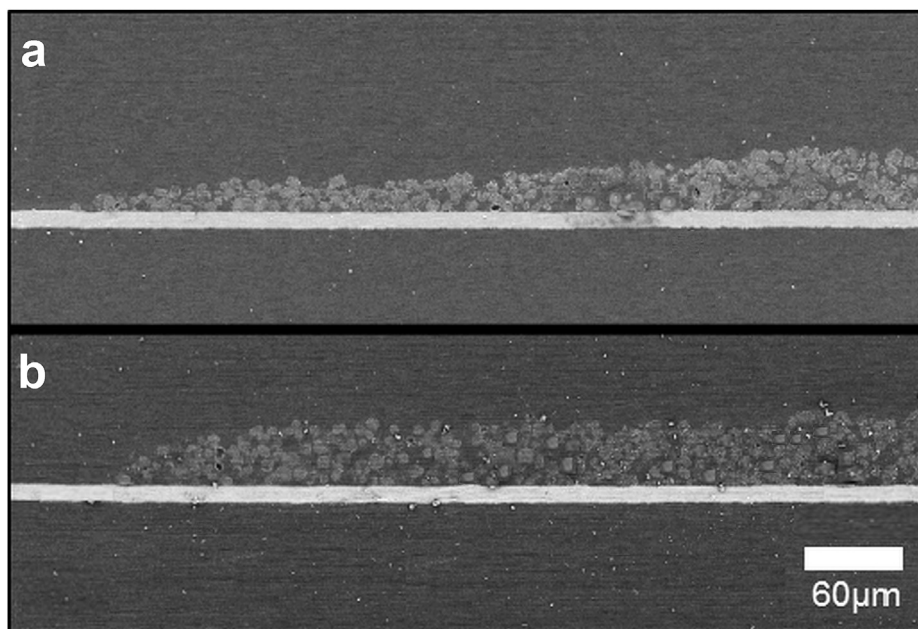


Fig. 14. SEM crosscut pictures of the edge area for a conventional slurry (a) ($\varphi_{\text{total}} = 20 \text{ vol\%}$, $\varphi_{\text{octanol}} = 0 \text{ vol\%}$) and a capillary suspension slurry (b) ($\varphi_{\text{total}} = 20 \text{ vol\%}$, $\varphi_{\text{octanol}} = 2 \text{ vol\%}$).

the failure is obviously located between the metal surface and the anode layer and not inside the anode layer. Slurries with differing solid fractions have been coated at a constant gap width of $300 \mu\text{m}$ onto copper foil using a doctor blade. In Fig. 12a the line load, which is defined as the peel force divided by the layer width, is shown for different coating layers obtained from capillary anode slurries as a function of the ball milling time after SBR addition. Obviously, thinner layers show higher force values during peeling which can be due to slower drying since the slurry contains a higher fluid fraction. As expected, samples without added SBR binder have low adhesion values. Already short kneading times between 5 and 15 min after SBR addition lead to a significant increase in line load. Surprisingly, longer kneading times resulted in weaker adhesion. Due to this finding, a kneading time of 10 min was chosen for the electrodes used for cell testing. In general, the electrodes made from capillary suspensions showed 20–30% lower adhesion strength compared to those made from regular suspensions (Fig. 12b). Presumably, octanol prevents the SBR from making contacts between the graphite particles and the copper substrate.

3.4. Edge contour characterization

Edge contours of wet electrode layers were analyzed using a 2D laser triangulation system. The investigated wet films were fabricated applying slot die coating, a common method in industrial Li-ion electrode manufacturing [20–23]. Using this coating method, the slurry is pumped through a die with a rectangular cross-section (Fig. 5) in which high shear rates ($\dot{\gamma}$) up to $10,000 \text{ s}^{-1}$ occur. At the outlet of the die a uniform distribution of fluid over the cross-section is achieved. With the help of a syringe pump the flow rate can be defined with high precision. Furthermore, the rotational speed of the backing roll is adjustable; as a result the layer thickness of the wet film can be controlled accurately. The laser triangulation sensor has been positioned at the top of the steel roll directly behind the slot die (as shown in Fig. 6) in order to detect the edge contour of the wet layer.

In Fig. 13, the wet film thickness at the edge of the coated layer is shown for two slurries differing in the addition of secondary fluid.

As it can be seen, the slurry based on a capillary suspension has a significantly sharper increase in layer thickness at the electrode side compared to the slurry without secondary fluid. This behavior can be explained with the differences in rheological properties: a good contour accuracy is achieved because of high viscosity values in the low shear region which prohibits spreading and flow due to gravitational force or surface tension. Furthermore, no superelevations were found for this slurry type. In contrast, the slurry without added secondary fluid does not maintain the shape of the coating instrument as accurately. This slurry flows even under the action of low gravitational stress or surface tension due to its low viscosity. Therefore the edge area, the transient region with rising layer thickness, is significantly larger compared to the capillary suspension. Moreover, superelevations of about $15 \mu\text{m}$ were detected for this slurry type during slot die coating.

Dried and calendered electrodes from different slurries exhibit similar differences in the edge shapes. In Fig. 14 SEM pictures of the side-edges of two electrodes are shown. In good agreement with the results for the wet films the electrode based on a capillary suspension has a characteristically sharp contour with a fast increase in thickness compared to the electrode fabricated from the conventional slurry. The angle of elevation characterizing the increase of the coating layer thickness perpendicular to the edge is by a factor of three higher for the electrode made from the capillary suspension compared to the one originating from the regular slurry.

3.5. Electrochemical characterization

The cycle performance of electrodes based on the two different slurry types is compared in Figs. 15 and 16. Cycling tests were executed with the anodes in three-electrode half cells against lithium at a C-rate of C/10 (Fig. 15). In addition, anodes were tested in Swagelok two-electrode half cells at varied C-rates against lithium (Fig. 16a) and 1C–1C cycling tests in full cells (Fig. 16b).

In Fig. 15, are reported the voltage vs. capacity curves for both anode types at a charge/discharge rate of C/10 for the first cycle (Fig. 15a) and for the second and third cycles (Fig. 15b). During the

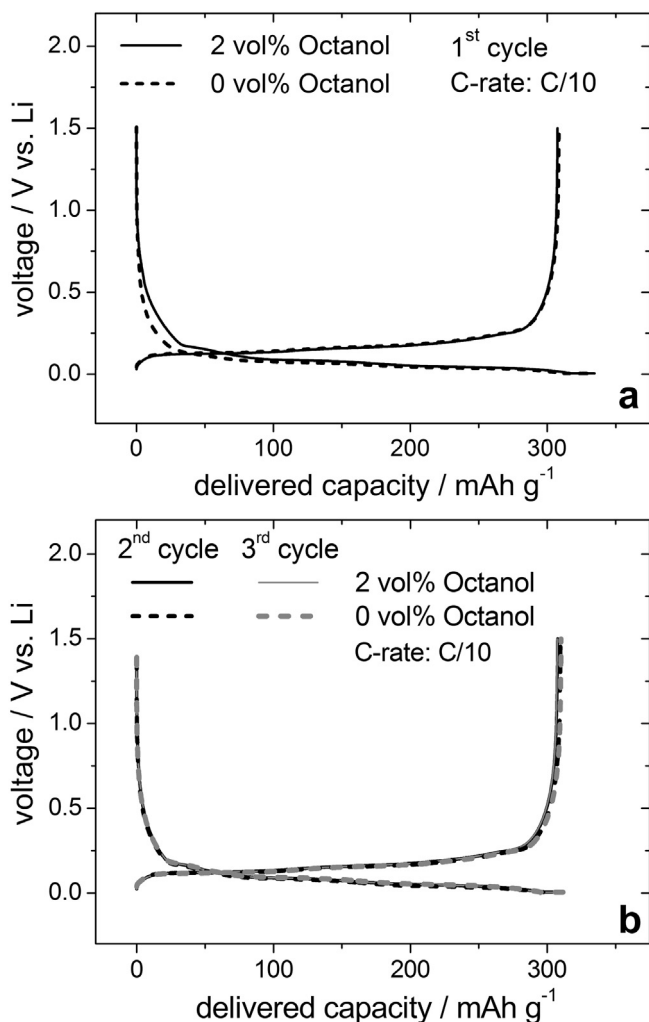


Fig. 15. Voltage profile vs. capacity for anodes made from a capillary suspension slurry ($\phi_{\text{total}} = 20 \text{ vol}\%$, $\phi_{\text{octanol}} = 2 \text{ vol}\%$) and a corresponding regular slurry ($\phi_{\text{total}} = 20 \text{ vol}\%$, $\phi_{\text{octanol}} = 0 \text{ vol}\%$) derived from cycling tests at a charging/discharging rate of C/10 in a half cell with lithium as counter and reference electrode. (a) First charge/discharge cycle, (b) second and third charge/discharge cycles.

first charging cycle a slight difference between both anode types in the voltage range between 0.7 and 0.1 V can be observed. The anode based on the slurry with added octanol shows a slightly higher irreversible capacity in comparison with the conventional anodes. This difference might be due to traces of octanol still present in the porous active material undergoing a reaction during the first charging cycle (more than 99% of the added octanol is evaporated during drying) resulting in a slightly lower efficiency value compared to the conventional anode (capillary suspension slurry: 91.9%, conventional slurry: 93.8%). During the first discharging cycle no differences between the two anodes are observable. Despite of this result for the first cycle, regarding the second and third charging/discharging cycles no differences are found for the two anode types (Fig. 15b). Obviously, no evidence for undesirable side reactions is observable after the first charging cycle, i.e. the electrodes perform similar after the first charging cycle.

In the two-electrode cell tests against lithium as counter-electrode we observed discharge capacity values of the cells close to the capacity of the material given by the supplier (310 mAh g⁻¹) at relatively low charging/discharging rates of C/10. With increasing C-rates the cells show a typical behavior of decreased capacity due to the high thickness (200 μm) of the glass fiber separator. Using

such types of separator the electrical resistance is increased as well as the diffusion limitation which explains the drop in capacity at higher C-rates [24]. No significant differences between the anodes based on the two slurry concepts are observable regarding the capacity during cell testing in half cells. The cell efficiency of both the electrodes is high and the relatively low capacity value for the first cycle can be explained with an irreversible capacity loss due to the SEI formation [25]. Furthermore, the cycling stability over 100 cycles was investigated in pouch cells against commercially available NMC-cathodes. Experiments were repeated five times for each anode with excellent reproducibility. The discharge capacity at 1C–1C charging/discharging in pouch cells is considerably higher compared to the tests in half cells. This can be explained by the lower thickness of the ceramic separator used in the pouch cell. Both electrodes show a good cycling stability over 100 cycles and a capacity loss of only about 2%.

Although during the first charging cycle differences could be observed for the two anode types, the addition of secondary fluid to the electrode slurry does not have a negative impact on the cycling stability. Therefore, the consequences of the octanol addition on the cycling behavior can be considered as negligible. Differences in the edge contour do not show up in the electrochemical properties of our cells since the edge areas had been cut-off during the cell assembling step, except for the take-off lug.

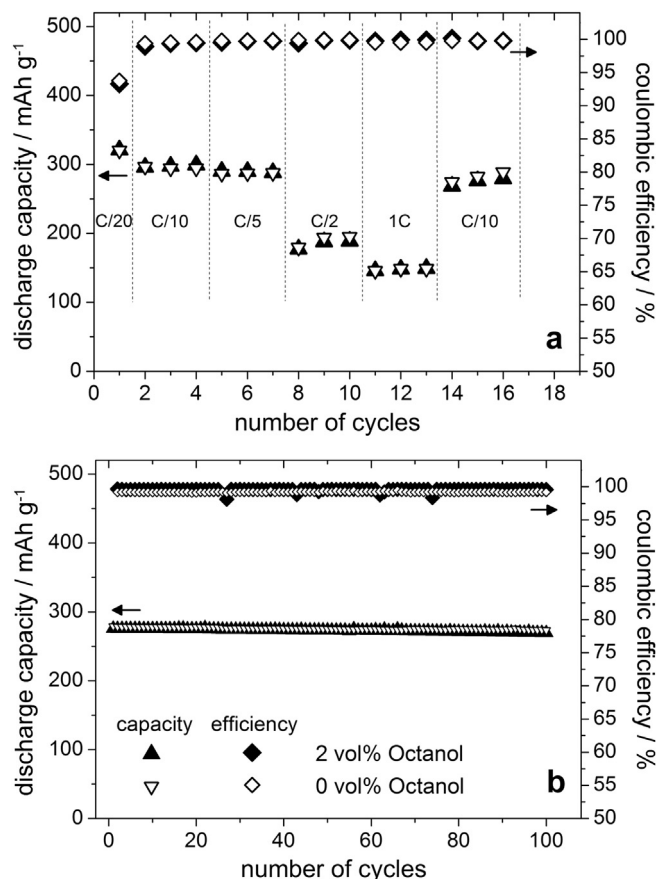


Fig. 16. Discharge capacity and coulomb efficiency values for electrodes made from a capillary suspension slurry ($\phi_{\text{total}} = 20 \text{ vol}\%$, $\phi_{\text{octanol}} = 2 \text{ vol}\%$) and a corresponding regular slurry ($\phi_{\text{total}} = 20 \text{ vol}\%$, $\phi_{\text{octanol}} = 0 \text{ vol}\%$) derived from cycling tests. (a) Results from tests executed against lithium as counter-electrode in Swagelok cells using a 200 μm thick separator. Tests were performed at different C-rates as indicated in the figure. (b) Results from cycling tests executed in pouch cells against commercially available NMC-cathodes at a charge-discharge rate of 1C–1C using a 30 μm thick separator (formation cycles at lower C-rates are not shown).

4. Conclusions

In this study, we introduce a novel slurry concept based on capillary suspensions for the fabrication of lithium-ion electrodes. Addition of a secondary fluid, immiscible with the main fluid of the suspension, can create a sample-spanning network controlled by capillary forces. This changes the rheological behavior of the suspension drastically, the low shear viscosity increases by orders of magnitude while the high shear viscosity remains unchanged.

The utilized secondary fluid evaporates during drying and does not remain in the electrode layer in contrast to conventional rheological additives.

Adjusting the rheological properties of the slurries by the use of capillary suspensions has beneficial consequences for the manufacturing of electrodes. Besides the improvement of the sedimentation stability, the coating behavior of slurries based on capillary suspensions is advantageous. High viscosity values in the low shear region result in superior edge contours and reduced cut-off waste. Since in industrial coating operations generally high shear stresses are applied and the flow properties in this range are not changed notably, established coating equipment can be used for processing slurries based on the novel formulation concept. Therefore, we consider its feasibility in industrial electrode fabrication as excellent.

The mechanical properties of layers based on capillary suspension slurries are sufficient and cycling stability tests confirmed that the new paste formulation concept has a negligibly negative impact, observable only during the first formation cycle, on the electrochemical properties.

Acknowledgements

We would like to acknowledge the Heinrich Böll foundation and the state Baden-Wuerttemberg for financial support. Thanks to Thomas Lebe for the work at the SEM microscope and the Institute for Applied Materials – Material Process Technology (KIT) for support in calendaring electrode layers. Further a special thanks to Jörg Kaiser and Madhav Singh from the Competence-E project (KIT)

and Andreas Flegler from Fraunhofer ISC for performing the cell tests. Part of this work has been supported by the Competence-E project at KIT.

References

- [1] H.Y. Tran, G. Greco, C. Täubert, M. Wohlfahrt-Mehrens, W. Haselrieder, A. Kwade, *J. Power Sources* 210 (2012) 276–285.
- [2] H. Zheng, L. Tan, G. Liu, X. Song, V.S. Battaglia, *J. Power Sources* 208 (2012) 52–57.
- [3] A.A. Tracton, in: *Coatings Technology Handbook*, third ed., CRC Press, Boca Raton, 2005.
- [4] K.M. Kim, W.S. Jeon, I.J. Chung, S.H. Chan, *J. Power Sources* 83 (1999) 108–113.
- [5] G. Lee, J. Ryu, W. Han, K.H. Ahn, S.M. Oh, *J. Power Sources* 195 (2010) 6049–6054.
- [6] J.H. Lee, U. Paik, V.A. Hackley, Y.M. Choi, *J. Electrochem. Soc.* 152 (2005) A1763–A1769.
- [7] J.H. Lee, S. Lee, U. Paik, Y.M. Choi, *J. Power Sources* 147 (2005) 249–255.
- [8] H. Buqa, M. Holzapfel, F. Krumeich, C. Veit, P. Novák, *J. Power Sources* 161 (2006) 617–622.
- [9] E. Koos, N. Willenbacher, *Science* 331 (2011) 897.
- [10] E. Koos, J. Dittmann, N. Willenbacher, *Chem. Ing. Tech.* 83 (8) (2011) 1305–1309.
- [11] E. Koos, J. Johannsmeier, L. Schwebler, N. Willenbacher, *Soft Matter* 8 (2012) 6620–6628.
- [12] E. Koos, N. Willenbacher, *Soft Matter* 8 (2012) 3988–3994.
- [13] M. Schmitt, P. Scharfer, W. Schabel, *J. Coat. Technol. Res.* 11 (1) (2014) 57–63.
- [14] B.P. Binks, J.H. Clint, *Langmuir* 18 (2002) 1270–1273.
- [15] R. Aveyard, B.P. Binks, J.H. Clint, *Adv. Colloid Interface Sci.* 100–102 (2003) 503–546.
- [16] C.O. Fournier, L. Fradette, P.A. Tanguy, *Chem. Eng. Res. Des.* 87 (2009) 499–506.
- [17] H. Schubert, *Powder Technol.* 37 (1984) 105–116.
- [18] M.E. Spahr, D. Goers, A. Leone, S. Stallone, E. Grivei, *J. Power Sources* 196 (2011) 3404–3413.
- [19] J. Dittmann, E. Koos, N. Willenbacher, *J. Am. Ceram. Soc.* 96 (2013) 391–397.
- [20] M. Yoshio, R.J. Brodd, A. Kozawa, *Lithium-Ion Batteries: Science and Technology*, Springer, New York, 2009.
- [21] S.F. Kistler, P.M. Schweizer, *Liquid Film Coating: Scientific Principles and Their Technological Implications*, Chapman & Hall, New York, 1997.
- [22] E.D. Cohen, E.B. Gutoff, *Modern Coating and Drying Technology*, Wiley, New York, 1997.
- [23] M. Schmitt, M. Baunach, L. Wengeler, K. Peters, P. Junges, P. Scharfer, W. Schabel, *Chem. Eng. Process. Process Intensif.* 68 (2013) 32–37.
- [24] G.H. Brilmyer, *J. Power Sources* 78 (1999) 68–72.
- [25] K. Striebel, K. Zaghbi, D. Guyomard, in: *Lithium and Lithium Ion Batteries: Proceedings, The Electrochemical Society, Pennington, 2004.*